External forces influence the elastic coupling effects during cargo transport by molecular motors

Florian Berger, Corina Keller, Stefan Klumpp, and Reinhard Lipowsky
Theory & Bio-Systems, Max Planck Institute of Colloids and Interfaces, 14424 Potsdam, Germany
(Received 1 September 2014; published 2 February 2015)

Cellular transport is achieved by the cooperative action of molecular motors which are elastically linked to a common cargo. When the motors pull on the cargo at the same time, they experience fluctuating elastic strain forces induced by the stepping of the other motors. These elastic coupling forces can influence the motors' stepping and unbinding behavior and thereby the ability to transport cargos. Based on a generic single motor description, we introduce a framework that explains the response of two identical molecular motors to a constant external force. In particular, we relate the single motor parameters, the coupling strength and the external load force to the dynamics of the motor pair. We derive four distinct transport regimes and determine how the crossover lines between the regimes depend on the load force. Our description of the overall cargo dynamics takes into account relaxational displacements of the cargo caused by the unbinding of one motor. For large forces and weak elastic coupling these back-shifts dominate the displacements. To develop an intuitive understanding about motor cooperativity during cargo transport, we introduce a time scale for load sharing. This time scale allows us to predict how the regulation of single motor parameters influences the cooperativity. As an example, we show that up-regulating the single motor processivity enhances load sharing of the motor pair.

DOI: 10.1103/PhysRevE.91.022701 PACS number(s): 87.16.Nn, 87.15.hj, 87.16.A−

I. INTRODUCTION

The complex internal structure of eukaryotic cells relies on an active transport system powered by motor proteins [1]. These molecular motors convert chemical energy into mechanical stepping by hydrolyzing ATP. Three families of motor proteins have been identified: myosins walking along actin filaments as well as kinesins and dyneins moving along microtubule tracks [2]. In muscles, millions of myosin motors form assemblies to cooperatively slide filaments [3,4], but cytoskeletal cargo transport is usually mediated by the cooperative action of a small number of motors belonging to the same or to different motor families [5–7]. Cargos transported by different motors can display complex motility patterns [8]. In the presence of both kinesins and dyneins, which walk in opposite directions, the movement of the cargo can be unidirectional or bidirectional. Both modes of transport can be interrupted by extended pauses [9]. However, the simplest case is transport by a team of identical motors [10,11]. Such systems have been studied in several *in vitro* experiments demonstrating the advantage of having more motors on a cargo: increasing the number of motors increases the overall run length of the cargo and the maximal force the motor team can generate [12–15]. In addition, in the presence of a load force the velocity of the cargo increases with the number of motors actively sharing the load [16]. On the other hand, recent experimental studies seem to suggest that load sharing is rather rare in the case of kinesin motors [17] and highly dependent on the type of motor and their interactions in living cells [18–20].

In the last couple of years, it became more and more evident that systematic studies of the dynamics of cargos transported by motor teams strongly contribute to our understanding of intracellular transport. Whereas the first experiments changed the number of motors in a rather unspecific manner by covering beads with motors [14,15,21], a more controlled method has been introduced recently based on the synthetic assembly of motors to DNA scaffolds [22]. Such synthetic scaffolds allow to construct a specific number of binding sites and even allow to bind different motors [23]. In several experiments, the interaction of two coupled kinesins has been addressed [22], also under external load forces [24]. Other experiments using DNA scaffolds have studied assemblies of two myosin V motors [25], two nonprocessive myosin Vc [26], several processive and nonprocessive kinesin motors [27], and a tug-of-war between dynein and kinesin motors [23].

Motivated by gliding assay experiments, early theoretical studies considered transport driven by a large number of motors [28,29]. About a decade ago, a rather general framework has been introduced to study transport by a small number of identical motors [10]. In this framework, the directed movement of the motors is described in a deterministic manner, but motor binding and unbinding as stochastic processes. Other studies included stochastic stepping and the geometry of the system [30–33]. However, these studies could not explain the experimental observations that two coupled kinesins pull each other from the filament, but move with a velocity that is close to the velocity of a single motor [22]. This interference effect has been studied theoretically by explicitly considering the coupling between the motors not only for kinesin, but also for dynein and myosin motors [11,17,34,35]. In general, depending on the single motor dynamics and the elastic coupling, motor pairs can exhibit four different transport regimes [11]. The emergence of these distinct regimes can be understood from intuitive time scale arguments that were derived for transport in the absence of an external load force [11,36].

In this article, we extend our description of two elastically coupled motors and include a constant external load force. This approach allows us to study the implication of such a force on the four different transport regimes. In contrast to previous studies, our description provides a rather general framework that can be applied to kinesin, myosin, and dynein motors. To intuitively understand how motors cooperate, we introduce a time scale for load sharing. If this time scale is larger than the time for spontaneous unbinding, the motors do not have enough time to reach a load-sharing configuration and, thus,

cooperate poorly. On the other hand, by increasing the single motor processivity, motors are able to share the load more frequently.

Our article is organized as follows. After a short review of our force-dependent single motor description, we consider a system of two elastically coupled motors under an external load. We first focus on two-motor runs, during which the cargo is actually pulled by both motors, and determine the average velocity and the average duration of these runs. By comparing three different time scales we identify four distinct transport regimes and discuss these regimes in the context of three different motor families as provided by kinesin, myosin, and dynein. Furthermore, we study the overall dynamics of cargo transport by two motors and introduce a time scale for load sharing which represents the relaxation time from an initial state, in which one motor carries the whole load, to a final state, in which the load is shared equally between the two motors.

II. ELASTICALLY COUPLED MOLECULAR MOTORS UNDER AN EXTERNAL LOAD

In the following, we consider cargo transport by two molecular motors and take their elastic coupling via the cargo explicitly into account. In addition, we study the influence of an external force acting on the cargo. Our theoretical description of two motors starts from the well-established single motor dynamics, which ensures consistency with the results of single motor experiments.

A. Single motor description

We consider a single motor as a stochastic stepper that moves forward with the force-dependent stepping rate $\alpha(F)$, unbinds from the filament with the force-dependent unbinding rate $\epsilon_1(F)$, and rebinds with the binding rate π. The stepping rate is determined by the experimentally accessible force-velocity relation $\mathcal{V}(F)$ according to $\alpha(F) = \mathcal{V}(F)/l$, where l is the step size of the motor. We take a load force opposite to the walking direction of the motor to be positive, whereas a negative force is an assisting force. For the sake of simplicity, we use a piecewise linear force-velocity relation that captures the response of a molecular motor to an external load as given by

$$\mathcal{V}(F) \equiv \begin{cases} v & \text{for} \quad F < 0 \\ v(1 - F/F_\mathrm{s}) & \text{for} \quad 0 \leqslant F \leqslant F_\mathrm{s}, \\ 0 & \text{for} \quad F > F_\mathrm{s} \end{cases} \tag{1}$$

where v is the force-free velocity and F_s the stall force at which the velocity vanishes.

For the force-dependence of the unbinding rate, we use the exponential form,

$$\epsilon_1(F) = \epsilon \exp(|F|/F_\mathrm{d}), \tag{2}$$

which depends on the force-free unbinding rate ϵ and the detachment force F_d. Note, that the absolute value of the force enters in the exponent which implies that we treat both directions in the same way.

Taken together, at a first step to understanding the interplay of stepping and unbinding of a motor team, we use a relatively simple force-velocity relation and a simple force-dependence of the unbinding rate, which nevertheless give insight into the cooperative transport behavior.

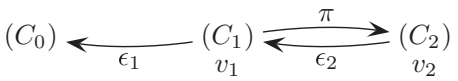

FIG. 1. Reduced state space of a cargo transported by two motors. Each cargo state is defined by the number of bound motors that pull on the cargo; in state (C_0) both motors are unbound, in state (C_1) and (C_2) one and two motors are bound, respectively. In the latter two states, the cargo is transported via one-motor and two-motor runs with velocity v_1 and v_2, respectively. Transitions between the states are described by the unbinding rates ϵ_1 and ϵ_2 and by the binding rate π.

B. Cargo transport by two motors

Because single motors bind and unbind from the filament, the number of motors pulling simultaneously on a cargo varies in time. After all motors have detached from the filament, the cargo diffuses away from the filament, which implies a finite run length of the cargo. This run length Δx_ca represents the distance along the filament that the cargo covers because of active transport by one or two bound motors. We distinguish these segments as one- and two-motor runs, during which the cargo is actively pulled by either one or two motors, respectively. The time during which the cargo is attached to the filament defines the binding or attachment time Δt_ca. Since binding and unbinding are stochastic processes, usually average values of the run length, $\langle \Delta x_\mathrm{ca} \rangle$, and the binding time, $\langle \Delta t_\mathrm{ca} \rangle$, are reported in experimental studies. To understand the relation between these quantities and the single motor parameters, theoretical studies describe the cargo by a discrete state space. Every state is defined by the number of motors bound to the filament. For a cargo transported by two motors, the reduced state space based on the number of motors that link the cargo to the filament is shown in Fig. 1. Transitions between the states correspond to binding and unbinding events with associated transition rates. While the single motor unbinding rate ϵ_1 as defined in Eq. (2) depends on the force F acting on this motor, we take the binding rate π to be constant and independent of the force. The effective unbinding rate ϵ_2 in Fig. 1 is defined as the inverse of the average run time of a two-motor run. The numerical values of these rates depend on the interaction between the motors [10,11,35,36]. Depending on the number of bound motors, the velocity of the cargo could, in general, be different. Therefore, we assign different velocities v_1 and v_2 to the states (C_1) and (C_2) that correspond to one-motor and two-motor runs.

C. Two active elastically coupled molecular motors under a constant force

The dynamics of the cargo actively pulled by only one motor is governed by the single motor behavior, therefore we focus on two-motor runs, during which both motors are simultaneously bound to the filament. We consider a constant external load force F_ex acting on the cargo. This situation can be realized in a force feedback trap, which exerts a constant

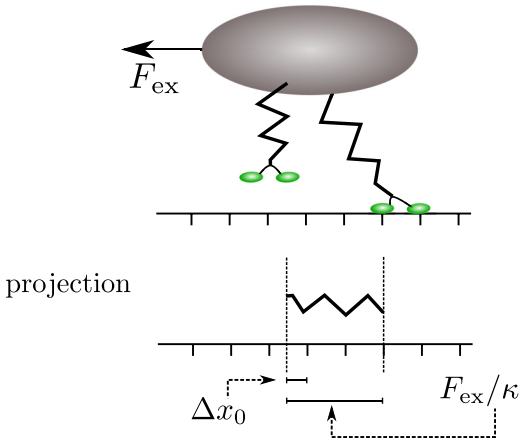

FIG. 2. (Color online) Cargo under an external load F_{ex} linked to the filament by one motor. The projection of the anchor point of the unbound motor need not match the lattice of the filament. In such a situation, the unbound, dangling motor cannot rebind into a "force-free" relaxed state. The mismatch between the projection of the anchor point and the closest binding site at the right is denoted by Δx_0.

load on the cargo. The motors are attached to the cargo via their elastic stalks, which we describe as linear springs with spring constant κ. In the following, we will use the intuitive terminology "motor stiffness" for this elastic parameter.

Initially, one motor is bound that sustains the total load force F_{ex}. In our one-dimensional description, this leads to a stretching of the motor by a distance of F_{ex}/κ; see Fig. 2. Next, we have to implement the binding process of the second motor to the filament. It is plausible to assume that this motor binds into a relaxed state and feels no load directly after rebinding. However, if the deformed spring of the first motor does not match the discrete lattice of the filament, the second motor cannot rebind into such a relaxed state. In the worst case this mismatch would be $\Delta x_0 = l/2$. Then, thermal fluctuations will push the motor to an adjacent binding site. After rebinding of the motor, the cargo relaxes to a new equilibrium position which is shifted by $\Delta x_0/2$. Note, that the factor $1/2$ arises from the fact that the cargo is bound to the filament by two motors that we consider as linear springs. This shift implies an extra force acting on the motors. However, for a realistic motor stiffness of $\kappa < 0.5\,\mathrm{pN/nm}$, the force is smaller 1 pN and thus smaller than the detachment force $F_d \simeq 3\,\mathrm{pN}$ and the stall force $F_s \simeq 6\,\mathrm{pN}$ for kinesin-1. Therefore, we neglect this additional effect and assume that the second motor always rebinds into a force-free state.

To describe this dynamical process, we consider a Markov process on a discrete state space, in which every state is associated with the discrete separation of the motors, resulting in a specific force; see Fig. 3. In the following, we explain this choice of a discrete force space in more detail. The unbound motor rebinds into state (0), in which the total load force F_{ex} acts on the other motor. Next, either the leading or the trailing motor steps forward, thereby stretching their elastic elements. We assume that the cargo relaxes fast to a new equilibrium position, $l/2$ away from the old position, and thus the forces on the motors are well defined. By every step the force on the motor is either increased or decreased by

$$F_K = \kappa l/2 \equiv Kl, \tag{3}$$

depending on the configuration; see Fig. 3. This equation defines the elastic coupling parameter K. A transition from state (j) to the next higher state $(j+1)$ corresponds to a forward step of the leading motor, bearing the load $F_{ex} + jF_K$, with stepping rate $\alpha(F_{ex} + jF_K)$. The transitions from state (j) to state $(j-1)$ occur by a forward step of the other motor with stepping rate $\alpha(-jF_K)$. After the unbinding of one motor, the cargo is transported by a single motor in state (C_1). Unbinding can occur from each state (j) with the transition rate

$$\omega_{off}(j) = \epsilon_1(F_{ex} + jF_K) + \epsilon_1(-jF_K). \tag{4}$$

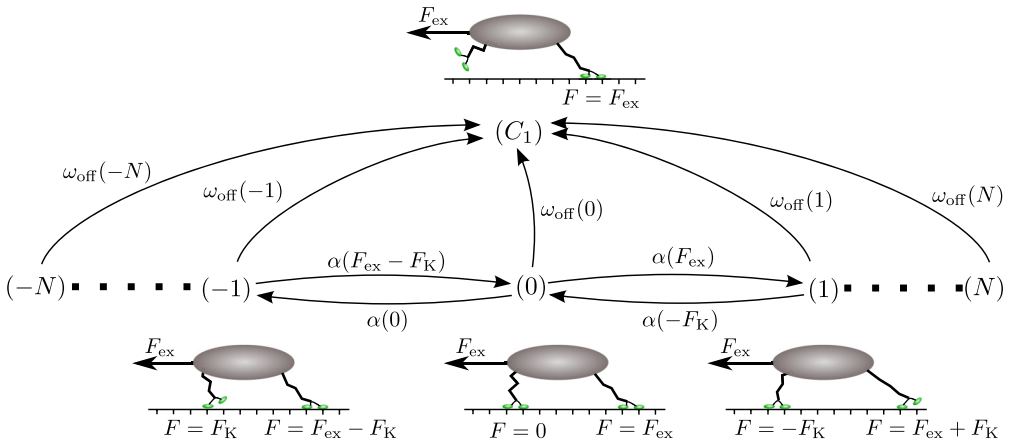

FIG. 3. (Color online) Network for two elastically coupled motors exposed to an external load force F_{ex}. Every state is associated with a certain force configuration. During one-motor runs in (C_1), the total force is sustained by the single bound motor. During two-motor runs, the two motors constantly redistribute the load force as a result of their stochastic stepping. Each step acts to stretch or relax the linkers of the motors resulting in an elastic force $F_K = \kappa l/2 = Kl$ [see Eq. (3)] contributing to the total force acting on each motor. In state (j) one motor is subjected to the force $F_{ex} + jF_K$ and the other motor to $-jF_K$. We implicitly assume that an unbound motor binds in a relaxed configuration to the filament bearing no load (the corresponding rebinding transition to (0) is not included in this figure). The forces in each state determine the stepping rates α and the effective unbinding rate ω_{off}.

Note, in the description above, the rates for a transition going out of a state only depend on the force of that state. Thus, we do not account for the change of the force during a transition. This simplification is justified for small coupling parameter K. In this case, the force generated per step is rather small. For large K, the stretching of the elastic elements between the motors by a single step could lead to a motor-motor force which is comparable to the stall force. A system with $\kappa = 2F_s/l$ would be so rigid that one step could stall the motor.

Using the discrete description introduced above, we want to obtain the binding time and the velocity of two motors simultaneously transporting a common cargo. The average time both motors are bound to the filament is the average time to absorption to state (C_1), initially started in state (0); see Fig. 3. To obtain this average time, we consider a closed network without the absorbing state and calculate the steady state probability distribution P_i, as proposed by Hill [37] and used in other studies [11,38]. Alternatively, the same time can be calculated by standard methods for Markov processes with absorption, sometimes called "first step analysis" [39]. The inverse probability current into the absorbing state gives us the average binding time

$$t_2 \equiv \left[\sum_j \omega_{\rm off}(j) P_j\right]^{-1}. \tag{5}$$

The velocity of the cargo transported by two motors is related to the average stepping rate as

$$v_2 \equiv (l/2)\sum_j [\alpha(F_{\rm ex} + jF_{\rm K}) + \alpha(-jF_{\rm K})]P_j. \tag{6}$$

In order to reduce parameters, we compare these two quantities to the corresponding single motor binding time $t \equiv \epsilon^{-1}$ and velocity v. We introduce the scaled binding time t_2/t and the scaled velocity v_2/v for two-motor runs.

Note that the definition of the velocity is an averaged stepping rate. It gives a value even if the motor only performs one step before unbinding. A situation that one could hardly observe in experiments would be provided by a load force that is much larger than the single motor stall force. For such a scenario, consider state (0) of Fig. 3. The leading motor is stalled by the large load force, but the trailing motor can step, which leads to a velocity of $l\alpha(0)/2$. If the leading motor unbinds immediately after one step, the two-motor run is terminated and its velocity would be $v_2 = l\alpha(0)/2$ independent of the external force. We discuss this extreme case in Sec. II F.

D. Scaled forces and transport regimes

The description of elastically coupled motors is based on three force scales: the detachment force $F_{\rm d}$, which is the force scale for force-induced unbinding, the stall force $F_{\rm s}$, which is the force scale for force-induced stalling, and the force $F_{\rm K}$, which is the elastic strain force induced per motor step. In addition to these forces, the external load force on the cargo $F_{\rm ex}$ provides a fourth force scale. The dynamical interplay of these forces dictates the transport properties. To develop an intuitive

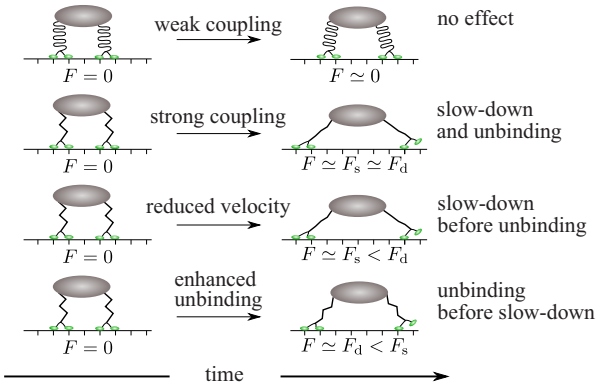

FIG. 4. (Color online) A load-free cargo transported by two elastically coupled motors can display four different transport regimes. These regimes depend on the elastic coupling strength between the two motors and their single motor parameters. In the weak coupling regime, no strain force is built up, and there is almost no effect on the velocity or the binding time. In contrast, for strong elastic coupling, and for $F_{\rm d} \simeq F_{\rm s}$ the force induced by the motors' stepping influences both the velocity and the binding time. However, if F_s is smaller compared to F_d, one motor will stall the other motor before one of the motors unbinds and the system exhibits the reduced velocity regime. Finally, if F_d is smaller compared to F_s, one motor will pull the other motor from the filament before the motors reduce their velocity, a behavior that characterizes the enhanced unbinding regime.

picture, it is convenient to scale all forces by the elastic coupling force $F_{\rm K}$. Doing so, we introduce a rescaled stall force $f_{\rm s} \equiv F_{\rm s}/F_{\rm K}$, a rescaled detachment force $f_{\rm d} \equiv F_{\rm d}/F_{\rm K}$, and a rescaled load force $f_{\rm ex} \equiv F_{\rm ex}/F_{\rm K}$. The calculation of the scaled quantities t_2/t and v_2/v now only involves, in addition to the three force scales, two time scales: the inverse force-free stepping rate $1/\alpha(0)$ and the inverse force-free unbinding rate $1/\epsilon$.

Previously, four distinct transport regimes have been identified theoretically for two cooperating molecular motors without an external force [11]: (i) *the weak coupling* regime with almost no effect on the binding time and the velocity, (ii) *the strong coupling* regime with a reduction of both, the binding time and the velocity, (iii) *the reduced velocity* regime with a reduced velocity but no effect on the binding time, and (iv) *the enhanced unbinding* regime with a reduced binding time but almost no effect on the velocity; see Fig. 4. As explained above, we are able to calculate the scaled velocity and scaled binding time as a function of the rescaled detachment and stall force $f_{\rm d}$ and $f_{\rm s}$ for different rescaled load forces $f_{\rm ex}$; see Fig. 5. Each corner of the plots correspond to a specific transport regime: in the upper part, for large $f_{\rm d}$, there is almost no effect on the binding time, whereas in the lower part the binding time is reduced. On the left side of the plots, for small $f_{\rm s}$, the velocity is reduced, while on the right side the velocity is comparable to the noninteracting case. As we increase the load force, the weak coupling regime (in the upper right corner) shrinks and the reduction in the binding time and/or the velocity increases. To describe the dependence of the regimes on the parameters, we estimate the crossover lines from the comparison of three different time scales.

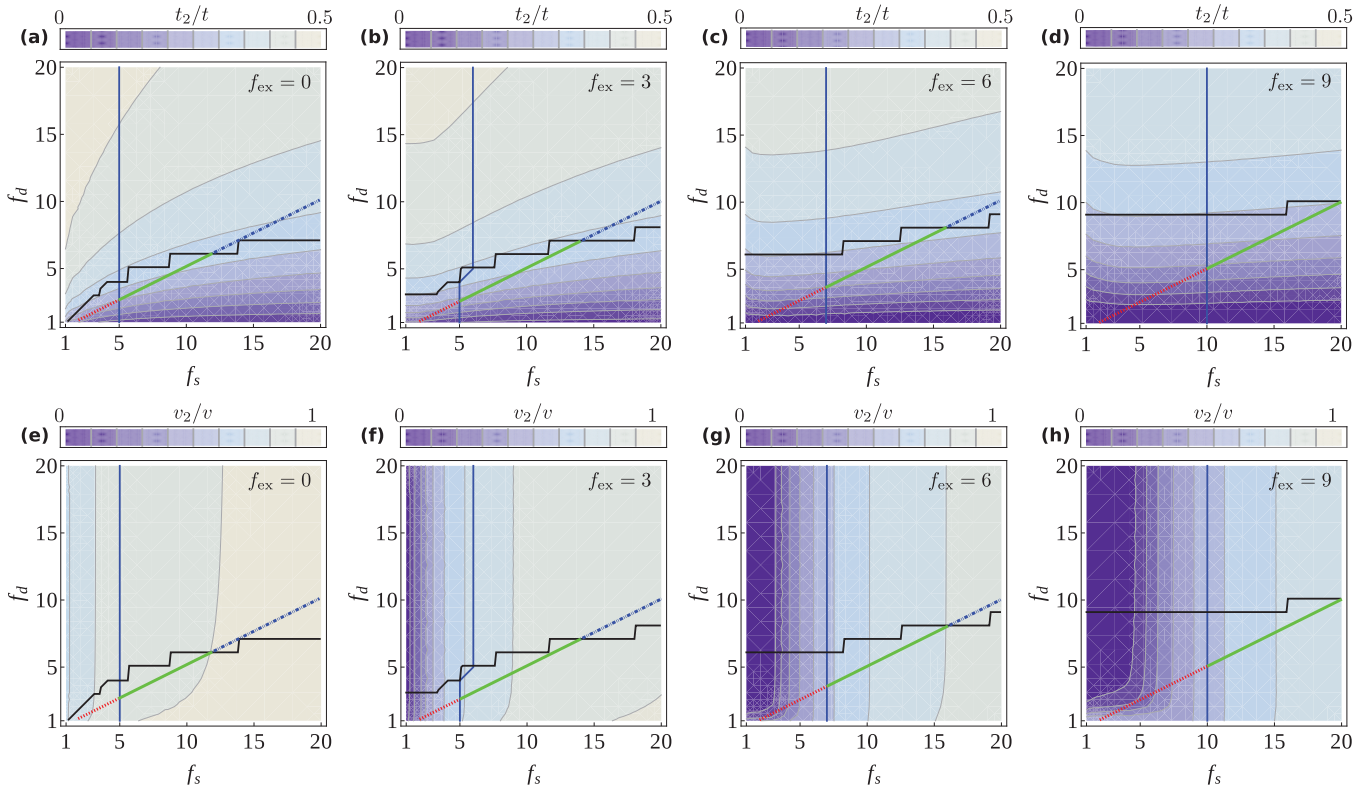

FIG. 5. (Color) (a–d) Binding time t_2 of two-motor runs in units of the single motor force-free binding time t. (e–h) Velocity v_2 of two-motor runs in units of the single motor force-free velocity v. Both quantities are displayed as a function of the scaled detachment force $f_d = F_d/F_K$ and the scaled stall force $f_s = F_s/F_K$ for different scaled load forces $f_{ex} = F_{ex}/F_K$; (a, e) $f_{ex} = 0$, (b, f) $f_{ex} = 3$, (c, g) $f_{ex} = 6$, (d, h) $f_{ex} = 9$. The solid black and blue lines are crossover lines between different transport regimes. The straight line corresponds to a pair of kinesin motors with a stall to detachment force ratio $F_s/F_d \simeq 2$. Along the latter line, the coupling parameter K and the force F_{ex} are changed in such a way that $f_{ex} = F_{ex}/lK$ remains constant. The different colored segments indicate the different transport regimes (from left to right): strong coupling (red), enhanced unbinding (green), and weak coupling (blue).

E. Different time scales

1. Time scale for spontaneous unbinding t_u

For two noninteracting motors that share the load equally, the time until one motor unbinds is given by

$$t_u \equiv [2\epsilon \exp(f_{ex}/2f_d)]^{-1}. \quad (7)$$

We call this time the time scale for spontaneous unbinding during equal load sharing.

2. Time scale for induced unbinding t_{F_d}

As the motors step asynchronously along the filament, they redistribute the load force and additionally build up a strain force by stretching the elastic elements between them. If the total force on a motor is comparable to the detachment force, it is very likely that the motor unbinds. To estimate the time scale t_{F_d} for such induced unbinding, we calculate the mean first passage time until one of the motors reaches a force that is comparable to the detachment force [11]. For this estimate, we neglect unbinding and use the modified network shown in Fig. 6. We promote the state (N_p), where $N_p = \lceil f_d - f_{ex} \rceil$ and (N_m), where $N_m = -\lceil f_d \rceil$ to absorbing states. Here, $\lceil x \rceil$ is the ceiling function that returns the smallest integer $\geq x$.

3. Time scale for reduced stepping t_{F_s}

In the case that the total force on a motor is comparable to the stall force, motor stepping is substantially slowed down. To estimate the time scale t_{F_s} for reduced stepping, we determine the mean first passage time until one of the motors reaches stall force. Again, we neglect unbinding and use the modified network shown in Fig. 6, but with the absorbing states corresponding to the stall force, $N_p = \lceil f_s - f_{ex} \rceil$ and $N_m = -\lceil f_s \rceil$.

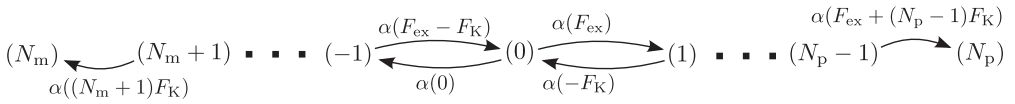

FIG. 6. Network to estimate two different time scales: (i) the time scale for induced unbinding, with $N_p = \lceil f_d - f_{ex} \rceil$ and $N_m = -\lceil f_d \rceil$ and (ii) the time scale for reduced stepping with $N_p = \lceil f_s - f_{ex} \rceil$ and $N_m = -\lceil f_s \rceil$.

4. Crossover lines

With these three time scales at hand, we are able to estimate the crossover lines between the four different transport regimes. Intuitively, if the time scale for spontaneous unbinding is the smallest, i.e., $t_u < t_{F_d}$ and $t_u < t_{F_s}$, the motors operate in the weak coupling regime. The motors unbind before developing a substantial strain force between them. The strong coupling regime, in which stepping and unbinding are influenced by the strain force, is characterized by a small time scale for induced unbinding and a small time scale for reduced stepping, i.e., $t_{F_d} \simeq t_{F_s} < t_u$. In case the time scale for reduced stepping is the only small time scale, i.e., $t_{F_s} < t_u$ and $t_{F_s} < t_{F_d}$, the strain force between the motors slow down stepping and the system is in the reduced velocity regime. The motors operate in the enhanced unbinding regime, if the time scale for induced unbinding is the smallest, i.e., $t_{F_d} < t_u$ and $t_{F_d} < t_{F_s}$. In this case force induced unbinding is the dominant process.

To compare the time scales obtained from the discrete state space shown in Fig. 6, we use the following simple definitions: (i) The crossover line between the stepping regimes is given by the smallest integer values of f_s and f_d for which $t_{F_s} \geq t_u$. (ii) The crossover line between the unbinding regimes is given by the smallest integer values of f_s and f_d for which $t_{F_d} \geq t_u$. These definitions determine well defined crossover lines indicated by the blue and the black line in Fig. 5, and it avoids difficulties that arise by considering the variable f_s and f_d continuously [11].

Increasing the scaled load force on the motors enhances the unbinding and reduces the velocity. This effect is captured by the shift of the crossover lines to higher rescaled stall and detachment forces; see Fig. 5.

5. Transport regimes for different motor species

For the binding time and the velocity shown in Fig. 5, we used the numerical values of the force-free stepping rate and the force-free unbinding rate of kinesin-1. In addition, fixing the stall force and detachment force to the kinesin-1 values of 6 pN and 3 pN respectively, the system is described by a straight line with the coupling parameter and the external load force as the only free parameters. Such lines are displayed in Fig. 5. The different colored segments indicate the different transport regimes: strong coupling (red), enhanced unbinding (green), and weak coupling (blue). Along the line, the coupling parameter K and the force F_{ex} are changed such that $f_{ex} = F_{ex}/lK$ is constant.

Some single motor parameters are also measured or estimated for motor species other than kinesin-1; see Table I. For each set of parameters, we calculate the binding time and the velocity as a function of the scaled stall and detachment forces together with the crossover lines between the transport regimes. Then, we fix the stall and detachment force and determine the intersection points between the straight line describing the system and the crossover lines. From this procedure we obtain for each motor pair a line which is subdivided in different segments corresponding to the different transport regimes; see colored segments in Fig. 7. Each point on the line represents a motor pair with a specific coupling parameter subjected to a certain load force. Inspection of such lines for different motor species and different scaled load forces reveal that all motors can operate in the strong and weak coupling regime. In addition to that, pairs of kinesin and of dyneins can access the enhanced unbinding regime, whereas myosin motors can work in the reduced velocity regime; see Fig. 7. As the scaled load force is increase on the motor pairs, the strong coupling regime is enlarged and the other regimes are shifted to higher scaled stall and detachment forces.

F. Transport by a pair of kinesin motors

We use the parameters given in the first column of Table I to describe transport by a pair of elastically coupled kinesin motors. In particular, we focus on the dynamics of two-motor runs. The scaled velocity v_2/v of two-motor runs as a function of external force is shown in Fig. 8(a) for different values of the motor stiffness κ. Increasing the elastic coupling between the motors slightly decreases the velocity for small external forces. In the limit of large external forces, the velocity reaches half of the force-free single motor velocity. In this case the most probable pathway is the following: one motor experiences the total load force and is stalled, the other motor binds in a force-free state performs one step with the rate $\alpha(0)$ and the cargo is displaced by $l/2$. Then, one of the motors unbinds from the filament and the two-motor run is terminated, resulting in a velocity of $l\alpha(0)/2$. These short trajectories are characterized by a small average scaled duration t_2/t and a small average displacement $\langle \Delta x_2 \rangle$ as shown in Fig. 8(b) and Fig. 8(c) for large F_{ex}. Interestingly, the velocity displays a minimum as a function of the external force; see Fig. 8(a). The appearance of the minimum can be understood according to the argument given above. If the second motor is able to catch up with the load bearing motor, both motors are slowed down. However, if the second motor unbinds before assisting the load-bearing motor, only fast steps of the second motor contribute to the overall velocity. As explained above, in the extreme case the latter motor only performs one step before unbinding again leading to half the single motor velocity.

The average duration t_2 of two-motor runs as a function of external force F_{ex} exhibits a maximum at $F_{ex} = F_K$; see

TABLE I. Values of the single motor parameters used to study the motor-motor interference of different pairs of elastically coupled motors. Kinesin-1_{Bl} and kinesin-1_{Di} indicate a set of parameters measured in different labs.

Parameter	Kinesin-1_{Bl}	Kinesin-1_{Di}	Strong dynein	Weak dynein	Myosin V	Myosin VI
Stall force F_s (pN)	6 [40,41]	7 [24,42]	7 [43]	1.1 [44]	2 [45]	2 [45]
Detachment force F_d (pN)	3 [41]	3 [41]	0.75 [9]	0.75 [9]	4 [45]	2.6 [45]
Velocity v (μm/s)	1 [41,42]	0.5 [22]	0.65 [9]	0.65 [9]	0.38 [45]	0.15 [45]
Unbinding rate ϵ (s^{-1})	1 [41]	0.61 [22]	0.27 [9]	0.27 [9]	0.3 [45]	0.25 [45]
Step size l (nm)	8 [42]	8 [22]	8 [43]	8 [43]	36 [45]	36 [45]

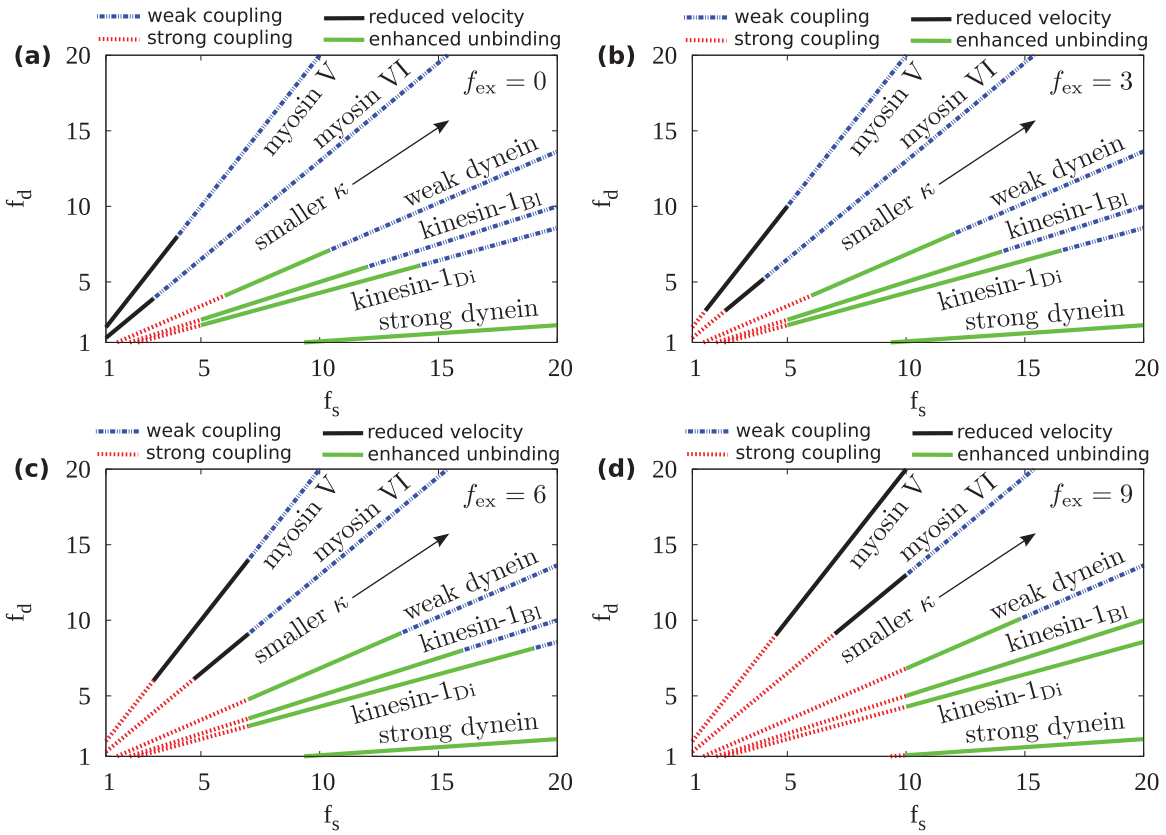

FIG. 7. (Color) Transport regimes for two elastically coupled motors simultaneously pulling on a cargo that is exposed to different load forces: (a) $f_{ex} = 0$, (b) $f_{ex} = 3$, (c) $f_{ex} = 6$, and (d) $f_{ex} = 9$. The lines correspond to different pairs of motors with single motor parameters given in Table I. The color-coded line segments represent the weak coupling (blue), the strong coupling (red), the reduced velocity (black), and the enhanced unbinding regimes (green).

Fig. 8(b). Inspection of the sum given in Eq. (5) reveals that the state $j = -1$ makes a dominant contribution and for $j = -1$ the rate given in Eq. (4) exhibits a maximum at $F_{ex} = F_K$.

III. OVERALL CARGO TRANSPORT BY MULTIPLE MOTORS

1. *Back-shifts*

Applying the theoretical framework presented above, we are able to determine v_2 and ϵ_2 in terms of the single motor parameters and the elastic coupling. Using these quantities, the network shown in Fig. 1 completely describes cargo transport by two motors [35].

For noninteracting motors, a displacement of the cargo is only caused by steps of the motors [10]. In contrast, when the motor stalks act as elastic springs, unbinding of a single motor leads to a new equilibrium position of the cargo and thus to a displacement; see Fig. 9 [46]. In the load-free case with $F_{ex} = 0$, these displacements cancel out on average, because the leading and the trailing motor then unbind with equal probability as follows from the symmetry relation $\epsilon_1(-F) = \epsilon_1(F)$ for the unbinding rate ϵ_1 given by Eq. (2). For $F_{ex} \neq 0$,

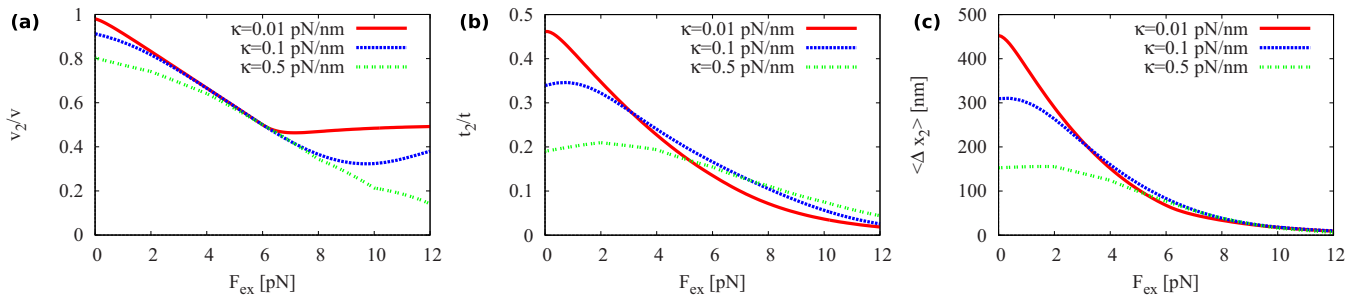

FIG. 8. (Color online) (a) Average velocity v_2 of two-motor runs in units of the single motor force-free velocity v, (b) Average duration t_2 of two-motor runs in units of the single motor binding time t and (c) average displacement $\langle \Delta x_2 \rangle$ of two-motor runs. All quantities are given as a function of the external load force F_{ex} for different values of the motor stiffness κ. As explained in the text, the two-motor runs consist of single steps for large values of F_{ex}. To describe the single motors, we used the kinesin parameters, $F_s = 6$ pN, $F_d = 3$ pN, $v = 1\,\mu$m/s, $\epsilon = 1\,s^{-1}$, $l = 8$ nm; see Table I.

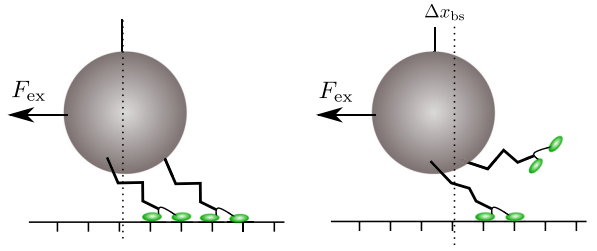

FIG. 9. (Color online) If the leading motor unbinds, the cargo relaxes to a new equilibrium position shifted by $\langle \Delta x_{bs} \rangle$. Such a back-shift contributes to the overall displacement of the cargo. A similar situation occurs when the trailing motor unbinds.

on the other hand, this symmetry is broken, since the force acts in a certain direction. To account for the resulting back-shifts, we explicitly consider the displacement of the cargo to a new equilibrium position after one of the motors has detached from the filament. This new position depends on the force and on the elasticity of the motor linkers. To determine the back-shifts, we proceed in three steps: (i) For each force state (j) of Fig. 3, we calculate the two displacements

$$\Delta x_{le}(j) \equiv -\frac{l f_{ex}}{2} - j\frac{l}{2} \tag{8}$$

and

$$\Delta x_{tr}(j) \equiv j\frac{l}{2} \tag{9}$$

corresponding to the relaxation of the cargo after the unbinding of the leading or trailing motor, respectively. (ii) We determine the average number of unbinding events per two-motor run for the leading and for the trailing motor from each state (j) of the network shown in Fig. 3. This average number is connected to the ratio of probability currents for the corresponding events [47], leading to the average number

$$\langle N_{le} \rangle(j) \equiv \frac{P_j \epsilon \exp(|f_{ex} + j|/f_d)}{\sum_j P_j \omega_{off}(j)} \tag{10}$$

of unbinding events for the leading motor from state (j). Likewise, for the trailing motor, we find the average number

$$\langle N_{tr} \rangle(j) \equiv \frac{P_j \epsilon \exp(|j|/f_d)}{\sum_j P_j \omega_{off}(j)} \tag{11}$$

of unbinding events from the same state. (iii) In a final step, we calculate for an overall cargo run, the average number $\langle N_2 \rangle$ of two-motor runs which is given by

$$\langle N_2 \rangle \equiv \frac{\pi}{\epsilon_1} = \frac{\pi}{\epsilon \exp[|f_{ex}/f_d|]} \tag{12}$$

as follows from the network shown in Fig. 1, because each cargo run starts in cargo state (C_1) [35].

Combining these results, we obtain the average displacement caused by back-shifts,

$$\langle \Delta x_{bs} \rangle \equiv \langle N_2 \rangle \sum_j [\langle N_{le} \rangle(j) \Delta x_{le}(j) + \langle N_{tr} \rangle(j) \Delta x_{tr}(j)]. \tag{13}$$

We then add this term as a correction to the overall cargo run length resulting in

$$\langle \Delta x_{ca} \rangle \equiv \frac{\pi v_2 + \epsilon_2 v_1}{\epsilon_2 \epsilon \exp[|f_{ex}/f_d|]} + \langle \Delta x_{bs} \rangle. \tag{14}$$

The overall cargo binding time is obtained from the network shown in Fig. 1 as

$$\langle \Delta t_{ca} \rangle \equiv \frac{\pi + \epsilon_2}{\epsilon_2 \epsilon \exp[|f_{ex}/f_d|]} \tag{15}$$

and the cargo velocity as

$$v_{ca} \equiv \frac{\langle \Delta x_{ca} \rangle}{\langle \Delta t_{ca} \rangle}. \tag{16}$$

In order to investigate whether the distinct transport regimes for two simultaneously pulling motors can be identified from the overall transport of the cargo, we plot the overall cargo binding time and the velocity; see Figs. 10(a)–10(d) and Figs. 10(e)–10(h), respectively. Indeed, we can associate the previously introduced transport regimes with each corner of the plots. Because of the back-shifts of the cargo, the velocity can be negative, even though our description neglects backward stepping of single motors. Another important quantity is the overall cargo run length which is plotted in Figs. 10(i)–10(l). For higher scaled load forces the run length decreases. It is interesting to notice that for example at a load force of $f_{ex} \simeq 3$, the maximum run length is around $f_d \approx f_s$. In Fig. 10, the colored line represents a pair of kinesin motors. The colored line segments indicate the different transport regimes: strong coupling (red), enhanced unbinding (green), and weak coupling (blue). The three different stars correspond to three systems with different motor stiffness $\kappa \simeq 0.075,\ 0.15,\ 0.5\,\mathrm{pN/nm}$. For these systems, the overall velocity, run time and run length of the cargo are shown in Fig. 11 as a function of load force. For large external forces, increasing the elastic coupling increases the cargo velocity. The binding time and the run length decrease when the elastic coupling is increased for small forces. Taken together, the elastic coupling that governs the strain forces between the motors has a different influence on the velocity, run length, and binding time.

Note that we do not use any arbitrary criteria to select trajectories. In contrast, only trajectories with a minimal length are often considered in experimental studies. Furthermore, the degree of cooperation depends on the rebinding rate π for which we took the literature value of $\simeq 5/\mathrm{s}$ [14]. This parameter will depend on the geometry and flexibility of the underlying molecular architecture.

IV. TIME SCALE FOR LOAD SHARING

The comparison of the different time scales in Sec. II E provides a conceptual framework to gain insight into the different transport regimes from an intuitive point of view. In order to develop an intuitive understanding of the cooperativity of motors under an external load, we now introduce a fourth time scale t_{sl} for load sharing. The time for load sharing is the time that is needed for two motors to share the external load, after the second motor has bound into the force-free state (0). This definition is motivated by the fact that load-sharing states

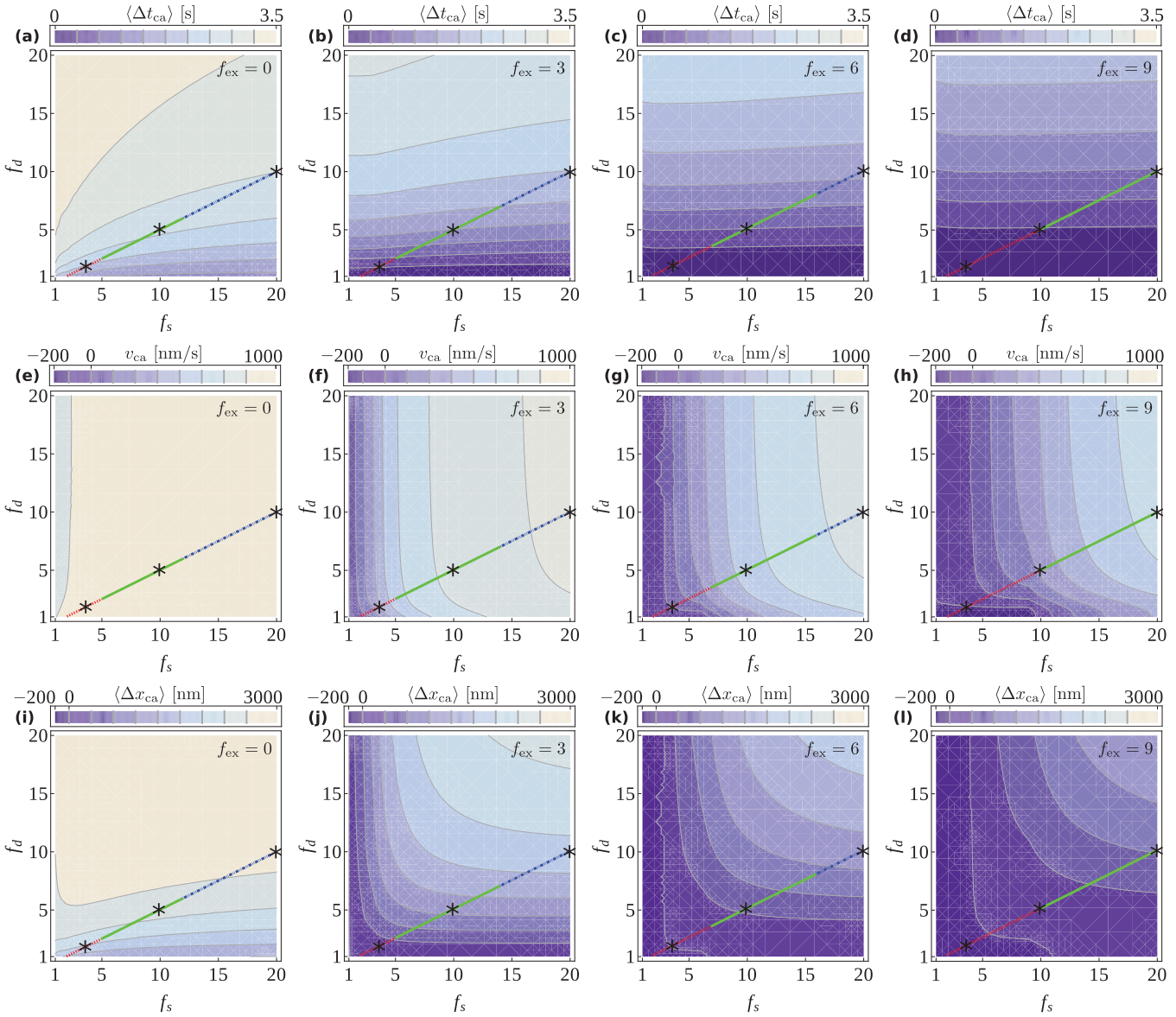

FIG. 10. (Color) (a–d) Overall binding time $\langle \Delta t_{ca} \rangle$, (e–h) overall average velocity v_{ca}, and (i–l) overall run length $\langle \Delta x_{ca} \rangle$ of a cargo transported by two motors as a function of the scaled detachment force f_d and stall force f_s for four different load forces f_{ex}. The straight lines correspond to a pair of kinesin motors with a stall to detachment force ratio $F_s/F_d \simeq 2$. Along the line, both K and F_{ex} are changed so that f_{ex} remains constant. The colored line segments indicate the different transport regimes (from left to right): strong coupling (red), enhanced unbinding (green), and weak coupling (blue). The three stars represent three different systems with fixed coupling strength and fixed external load force; see Fig. 11. When a motor unbinds, the cargo relaxes to a new position. For strong coupling and large loads, these back-shifts result in an effective backward displacement; see (k) and (l).

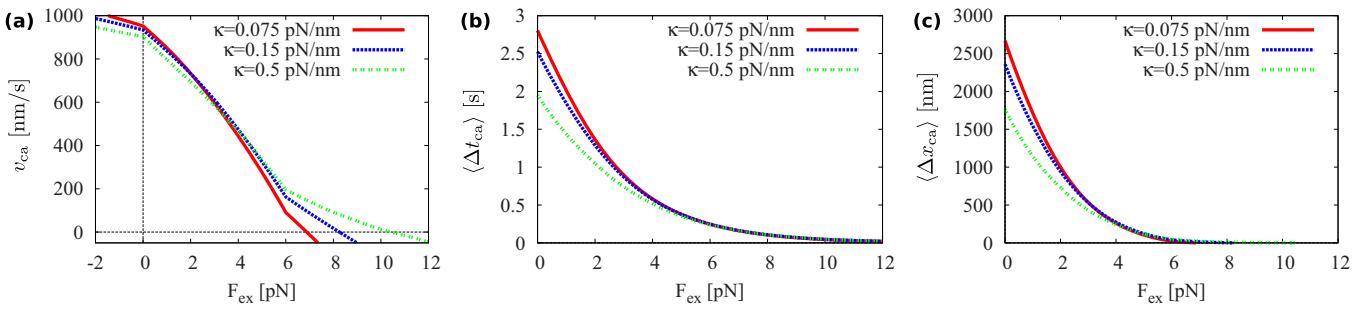

FIG. 11. (Color online) Velocity (a), binding time (b), and run length (c) as a function of the external load of a cargo pulled by two kinesin motors with parameter, $F_s = 6\,\mathrm{pN}$, $F_d = 3\,\mathrm{pN}$, $v = 1\,\mu\mathrm{m/s}$, $\epsilon = 1\,\mathrm{s}^{-1}$, $l = 8\,\mathrm{nm}$, $\pi = 5\,\mathrm{s}^{-1}$, and the elastic coupling $\kappa = 0.2\,\mathrm{pN/nm}$.

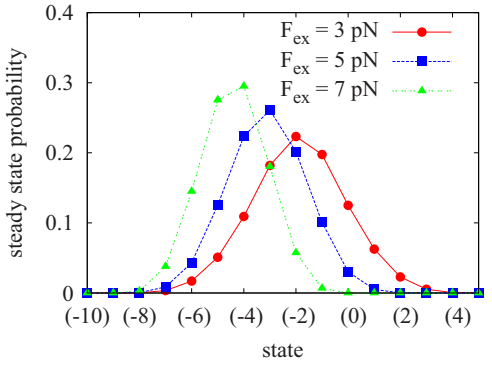

FIG. 12. (Color online) Steady state probability distribution of the network shown in Fig. 3 with $\omega_{\rm off}(j) = 0$ for all j. The peaks of the distributions correspond to states in which the force is shared almost equally between the motors. This example corresponds to two elastically coupled kinesins with parameters $F_{\rm s} = 6\,{\rm pN}$, $F_{\rm s} = 3\,{\rm pN}$, $\kappa = 0.2\,{\rm pN/nm}$, $l = 8\,{\rm nm}$, $v = 1\,\mu{\rm m/s}$, $\pi = 5\,{\rm s}^{-1}$, and $\epsilon = 1\,{\rm s}^{-1}$. The states are labeled as in Fig. 3.

are the most probable states of the steady state distribution for the network shown in Fig. 3 without unbinding. In Fig. 12 the steady state distributions for different external loads display maximums at states with negative indices which correspond to load-sharing states according to the network shown in Fig. 3. In mean field approaches, the load-sharing state has been used as the only state to describe motors under external forces [9,10].

We define the time scale for load sharing by the time that the system needs to relax to the steady state distribution shown in Fig. 12. We consider the network shown in Fig. 3 and set all unbinding rates $\omega_{\rm off}$ equal to zero. The master equation for such a system can be written in the form

$$\partial_t \mathbf{p} = \mathbf{M} \cdot \mathbf{p}, \tag{17}$$

where $\mathbf{p}$ is the vector containing the state probabilities and $\mathbf{M}$ is the transition rate matrix. The general solution for the initial state $\mathbf{p}_0$ is given by

$$\mathbf{p}(t) = \exp[\mathbf{M}t]\mathbf{p}_0, \tag{18}$$

with the steady state $\mathbf{p}_{\rm st} = \mathbf{p}(\infty)$. We define the time $t_{\rm sl}$ as the solution of the overlap criterion

$$\mathbf{p}(t_{\rm sl}) \cdot \mathbf{p}_{\rm st} \equiv \sum_i p_i(t_{\rm sl}) p_i(\infty) = 0.9. \tag{19}$$

This implicit equation can be easily solved numerically. By comparing this time scale to the spontaneous unbinding time $\epsilon_1^{-1}(F_{\rm ex})$ of a single motor bearing the total load, we predict whether motors are able to cooperate by sharing the load. Note that we now consider the spontaneous unbinding of a single motor, i.e., the motor that bears the total load initially [48]. If the the time $\epsilon_1^{-1}(F_{\rm ex})$ is large compared to the time for load sharing, the motors have enough time to distribute the load between them.

As an example, we calculate the time for load sharing by two coupled kinesin motors with motor stiffness $\kappa = 0.2$ pN/nm as a function of the external load and compare it to the spontaneous unbinding time of a single motor for two different force-free unbinding rates ϵ; see Fig. 13(a). The time $t_{\rm sl}$ for load sharing is independent of the single motor unbinding rate,

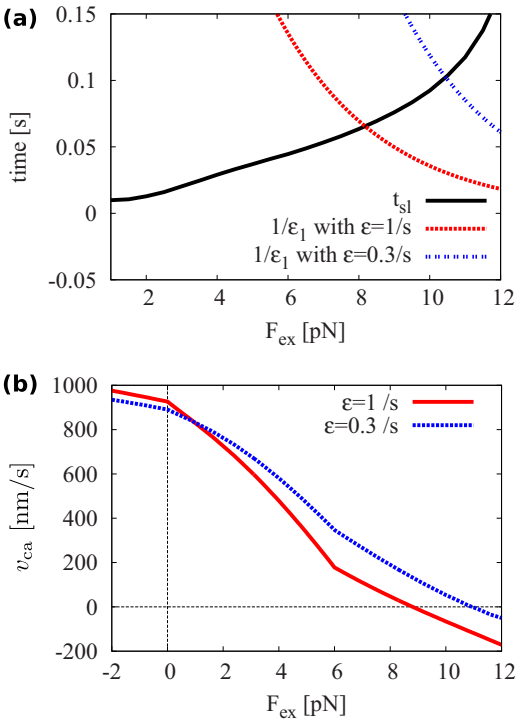

FIG. 13. (Color online) (a) Load-sharing time $t_{\rm sl}$ (black line) and unbinding time $\epsilon_1^{-1}(F_{\rm ex})$ (blue and red lines) for two coupled kinesins with parameters $F_{\rm s} = 6\,{\rm pN}$, $F_{\rm s} = 3\,{\rm pN}$, $\kappa = 0.2\,{\rm pN/nm}$, $l = 8\,{\rm nm}$, $v = 1\,\mu{\rm m/s}$, $\pi = 5\,{\rm s}^{-1}$, and $\epsilon = 1\,{\rm s}^{-1}$. For smaller force-free unbinding rates, the motors have more time to share the load and thus cooperate at higher load forces. This increased cooperativity leads to higher velocities for large forces; see (b). (b) Force velocity relation for a cargo transported by two kinesin motors with two different unbinding rates: $\epsilon = 1\,{\rm s}^{-1}$ (red), $\epsilon = 0.3\,{\rm s}^{-1}$ (blue).

because $t_{\rm sl}$ was calculated for $\omega_{\rm off} = 0$. For load forces $F_{\rm ex}$ with $t_{\rm sl} < \epsilon_1^{-1}(F_{\rm ex})$, motors are able to share the load. Motors with smaller unbinding rate $\epsilon \simeq 0.3$ /s cover a large force range, up to 11 pN, in which they are able to share the load. The higher degree of cooperation for a smaller unbinding rate is also reflected in a higher velocity under large forces; see Fig. 13(b). Therefore, the higher the processivity of the motors, the higher their ability to share the load. Similarly, equal sharing of a viscous force has been reported in a theoretical study, only when the processivity of the motors is increased [49].

V. DISCUSSION

We presented a stochastic description of two elastically coupled molecular motors under a constant external load force. The stochastic stepping of the motors induces a fluctuating force that affects their transport behavior. However, the precise influence of the external force on the transport depends on the single motor parameters and on the elastic coupling. To distinguish between the four transport regimes of weak coupling, enhanced unbinding, reduced velocity, and strong coupling, we compared three different time scales; see Sec. II E. Increasing the load force on the cargo decreases the weak coupling regime and enhances the regimes in which the motors interfere with each other. Furthermore, we introduced a fourth time scale for

the time to share the load, which describes how effectively motors cooperate and provides additional insight into their cooperative behavior from an intuitive point of view.

In order to obtain a small number of parameters, we used relatively simple expressions for the force-velocity relation, for the force-dependent unbinding rate, and for the elastic coupling. In the following, we will discuss possible extensions of these simplifications.

Our simple force-velocity relation captures the essential behavior of molecular motors. Indeed, it has been shown in experiments that the velocity is almost constant under assisting forces for different molecular motors such as kinesin [42], dynein [50], and myosin V [51]. As a further simplification, we neglected backward steps of the motors. For small forces, backward stepping is relatively rare for kinesin [42] and myosin V [52], but more frequent for dyneins [50,53,54]. Therefore, for dynein, there might be additional effects arising from back-stepping under large forces that we do not take into account for now.

The unbinding rate that we used in Eq. (2) is independent of the direction of the force. In general, the affinity of a motor to the filament may depend on the loading direction. An asymmetric unbinding behavior of the single heads could act to enhance the head-head coordination if the trailing head is more likely to unbind under a forward force than the leading head under a backward load. One study reported an asymmetric unbinding behavior for kinesin-1, in its nucleotide-free state [55]. In the case of dynein, there is also evidence for a catch bond behavior [56]. These more complicated functional dependencies for the unbinding rate can be easily included in our description via Eq. (4).

We described the elastic coupling between the motors as a linear spring. A linear spring behavior should usually apply for small forces, but nonlinear force extension relations could be possible and have been studied theoretically for the load free case in [36]. We considered a type of coupling between the motors in which the anchor points are fixed. Such a system could be realized with an DNA-origami [23,27] or with an antibody coupling exactly two motors to a single bead [57]. However, in the cell, when motors are attached to a membrane the coupling between them could be different, since the anchors are embedded in a fluid membrane. The force generation of multiple motors that pull a tube out of a membrane has been studied both experimentally [58,59] and theoretically [60]. Other types of coupling such as hydrodynamical coupling or coupling via a rigid backbone are discussed in Ref. [61].

In Ref. [17], it has been argued that detailed balance requires a force dependence of the binding rate. In contrast, our study is based on the view that all elastic elements of the motor relax, as soon as a motor under force unbinds from the filament. This relaxation deforms the free-energy landscape of the motor-filament bond, and rebinding is unlikely to follow the same reaction coordinate as unbinding. Therefore, we take the binding rate to be force-independent. Note that the overall binding process is rather complicated and depends on the molecular geometry [31], electrostatic interactions and other unknown factors. Different, more complicated binding behaviors could be studied using the time scale arguments introduced above. In particular, the time to share the load depends on the initial condition; see Eq. (19) and Eq. (18).

We based our study on an interaction between the motors that is mediated via their elastic linkers. Such a system could be studied experimentally using DNA-origami with optical or magnetic tweezers. If the transport is regulated by other proteins the basic mechanical interaction between the motors will still influence the dynamics. On the other hand, adapter proteins or other cofactors could in principle change the single motor parameters which will then alter the cooperative behavior. Such regulation might be a possibility for the cell to fine tune intracellular transport. Recently, it has been shown that decreasing the single motor velocity up-regulates the multikinesin run length [57,62]. As an example of regulation, in our study, we increased the ability to share a common cargo by increasing the processivity of the motors. The processivity factor dynactin is known to increase the run length of dynein [63]. Experiments with these components could provide a systematic way to study the regulation of cooperative transport and even construct an optimal system that maximizes certain transport properties. From this perspective, our framework elucidates how the single motor parameters influence the cooperative behavior and thus identifies the relevant components that provide promising candidates for regulation.

[1] J. Howard, *Mechanics of Motor Proteins and the Cytoskeleton* (Palgrave Macmillan, Sunderland, MA, 2005).

[2] M. Schliwa and G. Woehlke, Nature (London) **422**, 759 (2003).

[3] H. Huxley and J. Hanson, Nature (London) **173**, 973 (1954).

[4] A. F. Huxley and R. Niedergerke, Nature (London) **173**, 971 (1954).

[5] S. P. Gross, M. Vershinin, and G. T. Shubeita, Curr. Biol. **17**, R478 (2007).

[6] M. A. Welte, Curr. Biol. **14**, R525 (2004).

[7] E. Holzbaur, Curr. Biol. **20**, R641 (2010).

[8] F. Berger, C. Keller, M. J. Müller, S. Klumpp, and R. Lipowsky, Biochem. Soc. Trans. **39**, 1211 (2011).

[9] M. J. I. Müller, S. Klumpp, and R. Lipowsky, Proc. Natl. Acad. Sci. USA **105**, 4609 (2008).

[10] S. Klumpp and R. Lipowsky, Proc. Natl. Acad. Sci. USA **102**, 17284 (2005).

[11] F. Berger, C. Keller, S. Klumpp, and R. Lipowsky, Phys. Rev. Lett. **108**, 208101 (2012).

[12] D. L. Coy, M. Wagenbach, and J. Howard, J. Biol. Chem. **274**, 3667 (1999).

[13] S. M. Block, L. S. B. Goldstein, and B. J. Schnapp, Nature (London) **348**, 348 (1990).

[14] J. Beeg, S. Klumpp, R. Dimova, R. S. Gracià, E. Unger, and R. Lipowsky, Biophys. J. **94**, 532 (2008).

[15] R. Mallik, D. Petrov, S. A. Lex, S. J. King, and S. P. Gross, Curr. Biol. **15**, 2075 (2005).

[16] J. Gagliano, M. Walb, B. Blaker, J. C. Macosko, and G. Holzwarth, Eur. Biophys. J. **39**, 801 (2010).
[17] J. W. Driver, D. K. Jamison, K. Uppulury, A. R. Rogers, A. B. Kolomeisky, and M. R. Diehl, Biophys. J. **101**, 386 (2011).
[18] A. K. Efremov, A. Radhakrishnan, D. S. Tsao, C. S. Bookwalter, K. M. Trybus, and M. R. Diehl, Proc. Natl. Acad. Sci. USA **111**, E334 (2014).
[19] B. H. Blehm and P. R. Selvin, Chem. Rev. **114**, 3335 (2014).
[20] B. H. Blehm, T. A. Schroer, K. M. Trybus, Y. R. Chemla, and P. R. Selvin, Proc. Natl. Acad. Sci. USA **110**, 3381 (2013).
[21] M. Vershinin, B. C. Carter, D. S. Razafsky, S. J. King, and S. P. Gross, Proc. Natl. Acad. Sci. USA **104**, 87 (2007).
[22] A. R. Rogers, J. W. Driver, P. E. Constantinou, D. K. Jamison, and M. R. Diehl, Phys. Chem. Chem. Phys. **11**, 4882 (2009).
[23] N. D. Derr, B. S. Goodman, R. Jungmann, A. E. Leschziner, W. M. Shih, and S. L. Reck-Peterson, Science **338**, 662 (2012).
[24] D. K. Jamison, J. W. Driver, A. R. Rogers, P. E. Constantinou, and M. R. Diehl, Biophys. J. **99**, 2967 (2010).
[25] H. Lu, A. K. Efremov, C. S. Bookwalter, E. B. Krementsova, J. W. Driver, K. M. Trybus, and M. R. Diehl, J. Biol. Chem. **287**, 27753 (2012).
[26] L. K. Gunther, K. Furuta, J. Bao, M. K. Urbanowski, H. Kojima, H. D. White, and T. Sakamoto, Sci. Rep. **4**, 4907 (2014).
[27] K. Furuta, A. Furuta, Y. Y. Toyoshima, M. Amino, K. Oiwa, and H. Kojima, Proc. Natl. Acad. Sci. USA **110**, 501 (2013).
[28] S. Leibler and D. A. Huse, J. Cell Biol. **121**, 1357 (1993).
[29] F. Jülicher and J. Prost, Phys. Rev. Lett. **75**, 2618 (1995).
[30] A. Kunwar, M. Vershinin, J. Xu, and S. P. Gross, Curr. Biol. **18**, 1173 (2008).
[31] R. P. Erickson, Z. Jia, S. P. Gross, and C. C. Yu, PLoS Comput. Biol. **7**, e1002032 (2011).
[32] S. Bouzat and F. Falo, Phys. Biol. **7**, 046009 (2010).
[33] Z. Wang and M. Li, Phys. Rev. E **80**, 041923 (2009).
[34] J. W. Driver, A. R. Rogers, D. K. Jamison, R. K. Das, A. B. Kolomeisky, and M. R. Diehl, Phys. Chem. Chem. Phys. **12**, 10398 (2010).
[35] C. Keller, F. Berger, S. Liepelt, and R. Lipowsky, J. Stat. Phys. **150**, 205 (2013).
[36] F. Berger, C. Keller, R. Lipowsky, and S. Klumpp, Cell. Mol. Bioeng. **6**, 48 (2013).
[37] T. L. Hill, Proc. Natl. Acad. Sci. USA **85**, 2879 (1988).
[38] F. Berger, M. J. I. Müller, and R. Lipowsky, Europhys. Lett. **87**, 28002 (2009).
[39] N. G. V. Kampen, *Stochastic Processes in Physics and Chemistry* (Elsevier, Amsterdam, The Netherlands, 2011).
[40] K. Svoboda and S. M. Block, Cell **77**, 773 (1994).
[41] M. J. Schnitzer, K. Visscher, and S. M. Block, Nat. Cell Biol. **2**, 718 (2000).
[42] N. J. Carter and R. A. Cross, Nature (London) **435**, 308 (2005).
[43] S. Toba, T. M. Watanabe, L. Yamaguchi-Okimoto, Y. Y. Toyoshima, and H. Higuchi, Proc. Natl. Acad. Sci. USA **103**, 5741 (2006).
[44] R. Mallik and S. P. Gross, Curr. Biol. **14**, R971 (2004).
[45] M. Y. Ali, G. G. Kennedy, D. Safer, K. M. Trybus, H. L. Sweeney, and D. M. Warshaw, Proc. Natl. Acad. Sci. USA **108**, E535 (2011).
[46] C. Keller, Ph.D. thesis, University of Potsdam, 2012.
[47] T. L. Hill, Proc. Natl. Acad. Sci. USA **85**, 4577 (1988).
[48] In Sec. II E 1, in contrast, we were interested in the noninteracting case of equal load sharing and thus introduced a time scale involving both motors.
[49] C. B. Korn, S. Klumpp, R. Lipowsky, and U. S. Schwarz, J. Chem. Phys. **131**, 245107 (2009).
[50] A. Gennerich, A. P. Carter, S. L. Reck-Peterson, and R. D. Vale, Cell **131**, 952 (2007).
[51] A. E. Clemen, M. Vilfan, J. Jaud, J. Zhang, M. Bärmann, and M. Rief, Biophys. J. **88**, 4402 (2005).
[52] N. M. Kad, K. M. Trybus, and D. M. Warshaw, J. Biol. Chem. **283**, 17477 (2008).
[53] M. A. DeWitt, A. Y. Chang, P. A. Combs, and A. Yildiz, Science **335**, 221 (2012).
[54] W. Qiu, N. D. Derr, B. S. Goodman, E. Villa, D. Wu, W. Shih, and S. L. Reck-Peterson, Nat. Struct. Mol. Biol. **19**, 193 (2012).
[55] K. Kawaguchi, S. Uemura, and S. Ishiwata, Biophys. J. **84**, 1103 (2003).
[56] A. K. Rai, A. Rai, A. J. Ramaiya, R. Jha, and R. Mallik, Cell **152**, 172 (2013).
[57] J. Xu, Z. Shu, S. J. King, and S. P. Gross, Traffic **13**, 1198 (2012).
[58] G. Koster, M. VanDuijn, B. Hofs, and M. Dogterom, Proc. Natl. Acad. Sci. USA **100**, 15583 (2003).
[59] C. Leduc, O. Campàs, K. B. Zeldovich, A. Roux, P. Jolimaitre, L. Bourel-Bonnet, B. Goud, J. Joanny, P. Bassereau, and J. Prost, Proc. Natl. Acad. Sci. USA **101**, 17096 (2004).
[60] O. Campàs, Y. Kafri, K. B. Zeldovich, J. Casademunt, and J.-F. Joanny, Phys. Rev. Lett. **97**, 038101 (2006).
[61] T. Guérin, J. Prost, P. Martin, and J. Joanny, Curr. Opin. Cell Biol. **22**, 14 (2010).
[62] J. Xu, S. J. King, M. Lapierre-Landry, and B. Nemec, Biophys. J. **105**, L23 (2013).
[63] S. J. King and T. A. Schroer, Nat. Cell Biol. **2**, 20 (2000).